07

Analysis and control of terahertz radiation parameters in the CoFeB/(Pt, W, Ta) structures

© A.V. Gorbatova[1], P.Yu. Avdeev[1], E.D. Levedeva[1], A.M. Burjakov[1], N.V. Bezvikonny[1], N. Tirselen[2], V.L. Preobrazhensky[1,3], E.D. Mishina[1]

[1] MIREA - Russian Technological University, Moscow, Russia
[2] University Lille, CNRS, Centrale Lille, University Polytechnique Hauts-de-France, Lille, France
[3] Prokhorov Institute of General Physics, Russian Academy of Sciences, Moscow, Russia
E-mail: gorbatova@mirea.ru

Received May 24, 2024
Revised June 23, 2024
Accepted June 27, 2024

This paper presents the results of studying a series of spintronic terahertz emitters based on bilayer structures consisting of layers of ferromagnetic $Co_{20}Fe_{60}B_{20}$ and heavy metals Pt, W, and Ta. The structures were fabricated in one and the same process cycle on a common substrate. The results confirm that the mechanism of terahertz generation in the investigated series is related to the inverse spin Hall effect. It is shown that the terahertz emitter with a non-magnetic Pt layer produces terahertz radiation with an amplitude an order of magnitude higher than that in structures based on W and Ta, which is due to a larger spin Hall angle. In addition, the study has demonstrated the possibility of controllable manipulation of the terahertz radiation polarization in the developed series by using external magnetic field applied in the direction of the hard magnetization axis.

Keywords: terahertz radiation, spintronic emitter, inverse spin Hall effect, spin Hall angle, magnetic anisotropy.

DOI: 10.61011/TPL.2024.10.59702.20001

Terahertz (THz) radiation ($\sim 0.1-30$ THz) exhibits unique properties making it promising for a large number of applications [1–3]. Regardless of a significant progress in THz technologies, creation of efficient, inexpensive and compact THz radiation sources still remains a relevant task. Recent discoveries in the field of THz spintronics have led to creating conceptually and technologically simple spintronic THz emitters (STEs) based on structures made of ferromagnetic (FM)/non-magnetic (NM) materials [4]. The STE operation is based on the processes of ultrafast laser-induced demagnetization in FM films [5,6] and spin-charge transformation: inverse spin Hall effect (ISHE) [5,7] and inverse Rashba–Edelshtein effect [8]. STEs are characterized by high efficiency and wide range of operating frequencies [9]; they also open up new opportunities for controlling the THz radiation polarization, amplitude and frequency [10–12]. A significant part of the currently performed studies is devoted to optimizing the STE design so as to achieve maximum efficiency of THz generation [7,13,14]. At the same time, one of the STE advantages is the possibility to control the THz radiation characteristics, e.g. polarization, by using magnetic fields. Development of controllable STEs implies providing the necessary magnetic characteristics of spintronic structures. For instance, an efficient tool for rotating the polarization in a wide angle range are structures with uniaxial magnetic anisotropy whose magnetization perpendicular to the anisotropy axis leads to spin reorientation and rotation of THz polarization in a wide range of angles [10,11].

This paper presents the results of studying the THz radiation emission from a set of THz emitters based on bilayer FM/NM structures fabricated in one and the same technological cycle on a common substrate. The main goals of the study were as follows: (i) obtaining comparative data on the THz emission efficiency in structures with various NM layers (Pt, W and Ta); (ii) analysis of the THz generation mechanisms in the set of emitters under study;(iii) creation of uniaxial magnetocrystalline anisotropy in FM layers of the structures under consideration for the purpose of controlling the THz radiation polarization; (iv) investigation of the structuresмagnetic characteristics (magnetic THz-hysteresis loops, coercivity, anisotropy fields).

Magnetic structures were grown on a sapphire substrate by cathode sputtering at a LEYBOLD Z550 setup. To create uniaxial magnetic anisotropy in the plane of the structure, the $Co_{20}Fe_{60}B_{20}$ FM film 1.8 nm thick was deposited in magnetic field from a target with the same stoichiometric composition. The substrate surface was divided into four sections. In three sections there were fabricated bilayer FM/NM structures containing non-magnetic metals of three types (Pt, W and Ta); the NM layers were 1.8 nm thick. The fourth section was a single-layer $Co_{20}Fe_{60}B_{20}$ structure free of a non-magnetic layer. Thicknesses of ferromagnetic and non-magnetic materials were selected based on the research results presented in [7]. The authors have demonstrated that in the case of a bilayer STE the emitted THz pulse amplitude reaches its maximum at the total structure thickness of ~ 3.6 nm. The sample schematic view is given in Fig. 3, *a*.

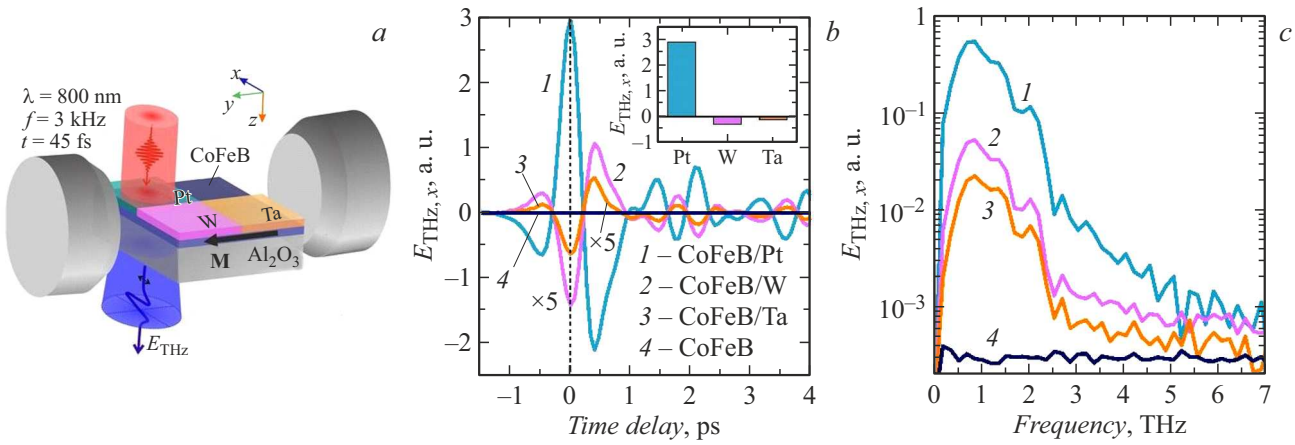

Figure 1. *a* — schematic diagram of the experimental sample and geometry of the THz spectroscopy experiment time-resolved from the laboratory frame of reference *xyz*. *b* — time dynamics of THz radiation generated by spintronic emitters under the applied external magnetic field of +2 kOe. The inset presents a histogram illustrating the dependence of maximum amplitude of the generated THz radiation (for the delay time of 0 ps) on the NM layer material. *c* — frequency spectra of generated THz pulses obtained by the Fourier transform method.

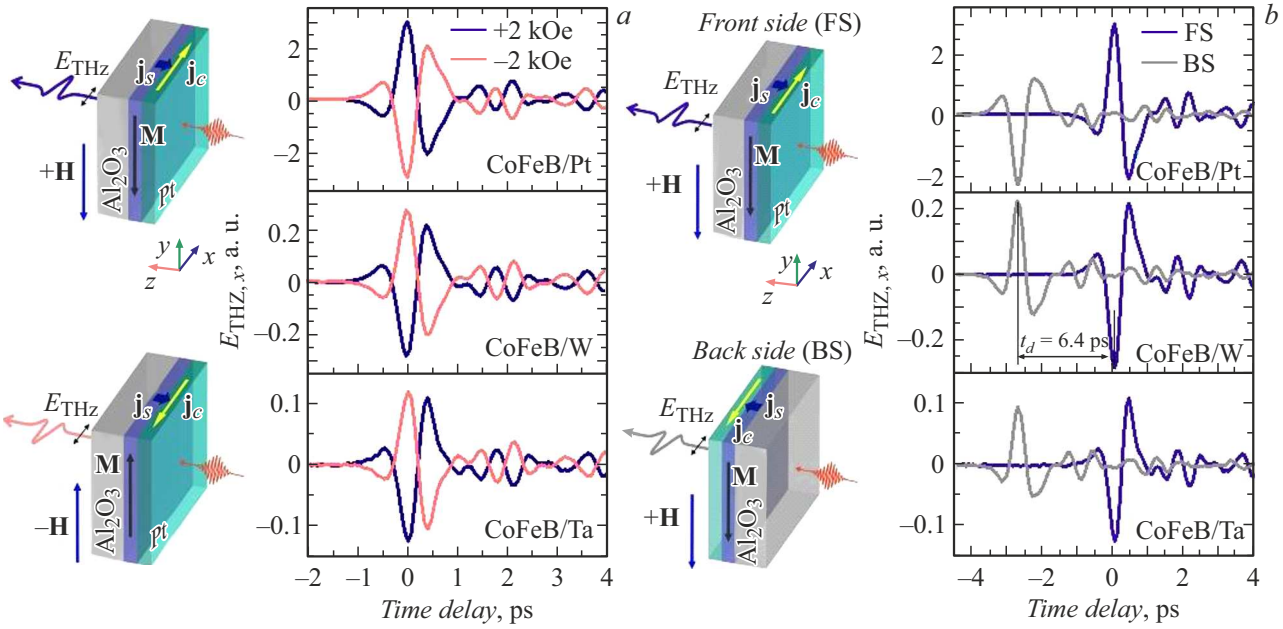

Figure 2. Analysis of the THz generation mechanisms in bilayer CoFeB/(Pt,W,Ta) structures. *a* — investigation of the effect of the external magnetic field **H** polarity on the THz signal temporal dynamics; *b* — investigation of the effect of direction of the structure irradiation with a laser pulse on the generated THz signal phase under the applied magnetic field with the same polarity.

Parameters of the THz radiation generation in the FM/NM structures were studied by using time-resolved „transmission“THz spectroscopy. Detailed description of this technique is given in [10]. Fig. 1, *b* presents temporal shapes of THz pulses generated by the CoFeB/(Pt,W,Ta) structures. THz signals were measured in the geometry with external magnetic field **H** 2 kOe in strength applied along the easy magnetization axis (E.A. is the„easy“ axis). The laser pump energy density was 0.5 mJ/cm^2, with the Gaussian beam full width at half-maximum of 1.28 mm. As Fig. 1, *b* shows, the greatest THz peak-to-peak amplitude (the difference between the maximum and minimum amplitude values) was observed for the CoFeB/Pt structure; its value was 17 and 22 times higher than those for CoFeB/ W and CoFeB/Ta, respectively. Reversal of the THz signal sign for W— and Ta-based emitters with respect to those with Pt (the inset to Fig. 1, *b*) is caused by the difference in the spin Hall angle signs.

The THz signal amplitude for the CoFeB FM film failed to be detected (Fig. 1, *b*). We relate the absence of this signal to the fact that the main mechanism of THz generation in ferromagnetics (such as Co, CoFeB,

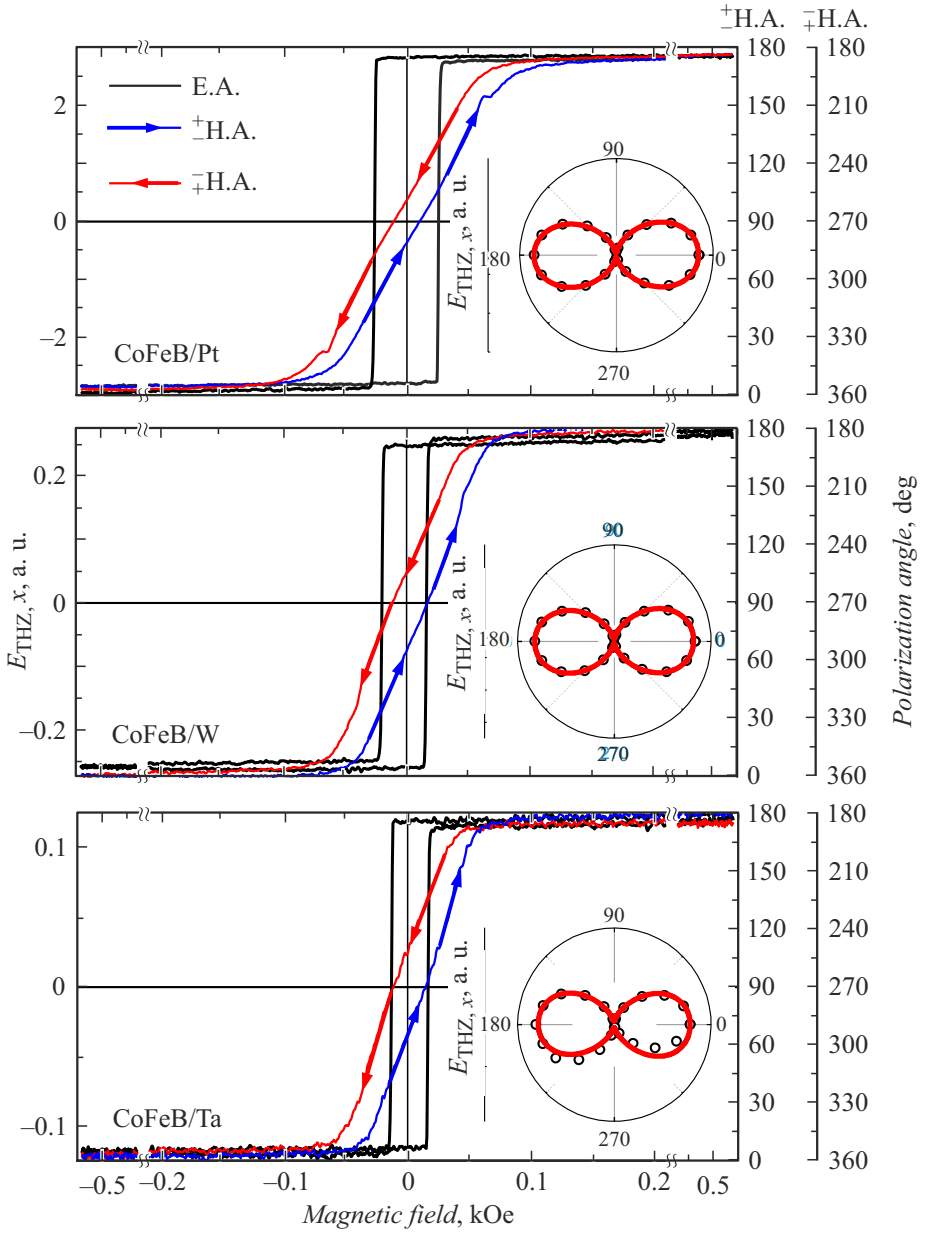

Figure 3. Magnetic hysteresis loops of the THz signal in the CoFeB/(Pt,W,Ta) structures. The insets present polarization-angle dependences of the THz amplitude E_x, which have been measured in the magnetic field of +2 kOe by rotating the THz polarizer.

etc.) is associated with the effect of ultrafast laser-induced demagnetization [15,16]. This mechanism is clearly pronounced for thick (~ 10 nm) FM films and is almost fully non-manifestable in ultrathin films [17]. Fig. 1, *c* presents the frequency spectra obtained by fast Fourier transform of temporal THz signals. The detected THz frequency range does not exceed 5 THz, being limited by the sensitivity threshold of the ZnTe detector crystal 200 μm thick.

Studies performed at the next stage allowed relating the THz radiation generation by the structures under consideration to the ISHE mechanism. Charge current $\mathbf{j}_c$ arising in the NM layer due to ISHE is defined as $\mathbf{j}_c \propto \theta_{SH}[\mathbf{j}_s \times \mathbf{M}]$, where θ_{SH} is the spin Hall angle of the NM film, $\mathbf{j}_s$ is the spin current propagating from the FM film to the NM layer, bf M is the unit magnetization vector of the FM-film. The charge current direction determines polarization of the generated THz wave.

We have analyzed the influence of direction of the external magnetic field oriented in the FM film plane on the THz wave polarization (phase) (Fig. 2, *a*). As Fig. 2, *a* shows, variations in polarity of the magnetic field of ± 2 kOe are accompanied by inversion of the THz wave phase, which confirms the spin nature of the generated THz radiation. Then the sample was rotated by 180° about the *y* axis of the laboratory frame of reference (Fig. 2, *b*). Changeover of the

sample side irradiated by the laser pulse is accompanied by a change in the direction of the spin current propagation from the FM— to NM-layer. As a result, inversion of the THz pulse phase takes place (Fig. 2, *b*). Time delay $t_d = 6.4$ ps between THz pulses generated for two different sample orientations relative to that of laser pumping is caused by the difference in speeds of the optical and THz beams propagation in the materials of the substrate and metal films.

Fig. 3 demonstrates the THz-signal magnetic hysteresis loops obtained by measuring the dependence of the THz signal amplitude (for $t_d = 0$ ps in Fig. 2, *a*) on external magnetic field in the CoFeB/(Pt,W,Ta) structures. The magnetic hysteresis loops were measured in two configurations: with the magnetic field applied along the easy magnetization axis (E.A.) and along the hard magnetization axis (H.A. that is the „“ axis). Projection of the THz radiation electric field onto axis *x* in the laboratory frame of reference was measured. The obtained THz signal hysteresis reflects variations in direction of the THz-radiation polarization in the angle range of $\pm 180°$ due to the magnetic moment rotation in the FM film plane, which is controlled by the external magnetic field [10].

As follows from the obtained hysteresis loops, coercive field H_c for structures with Pt, W and Ta is 26, 18 and 15 Oe, respectively. Magnitudes of saturation field H_s for the CoFeB/(Pt,W,Ta) structures are ~ 125, 100 and 50 Oe, respectively. The presence of the pronounced hard magnetization axis allows us to speak about the possibility to precisely control the THz polarization by external magnetic field in the low magnetic field range of -100 to 100 Oe by the method demonstrated in [10,11].

The Fig. 3 insets present the THz-signal angular dependences obtained by rotating the THz polarizer installed in the THz beam path under the applied magnetic field of 2 kOe. The position corresponding to 0° on the angular diagrams corresponds to the position of the THz polarizer maximally transmitting *x* component of the THz field. Angular dependences (red curves; the color version of the figure is given in the article electronic version) were approximated by the method described in detail in [11,18]. Good agreement between the experimental and approximation results allowed us to conclude that the THz polarization in the saturation state is linear.

Thus, the THz emission efficiency has been shown to depend on the NM layer material and spin Hall angle; the highest efficiency is exhibited by the structure with Pt. The main THz generation mechanism is ISHE; this has been confirmed by observing the THz-signal phase inversion with changover of the external magnetic field polarity and variation in the sample orientation with respect to the exciting wave propagation direction. The absence of a THz signal in the case of a single-layer CoFeB film is explained by that the main THz generation mechanism associated with ultrafast laser-induced demagnetization does not manifest itself in ultrathin films (1.8 nm). We have demonstrated the possibility of precisely varying the THz polarization in the range of -180 to 180° by using the external magnetic field. The control procedure is highly energy efficient: coercive field H_c does not exceed 26 Oe, while saturating fields H_s and anisotropy fields H_a do not exceed 100 Oe. In this paper, the results obtained for the studied structures have been explained within the ISHE model; they are in qualitative agreement with available experimental data obtained by other authors, and can serve as a guide in developing spintronic THz emitters with controllable parameters.

Funding

The study was supported by the Russian Science Foundation (project № 23-19-00849).

Conflict of interests

The authors declare that they have no conflict of interests.

References

[1] Y. Peng, C. Shi, X. Wu, Y. Zhu, S. Zhuang, BME Front., **2020**, 2547609 (2020). DOI: 10.34133/2020/2547609
[2] W. Jiang, Q. Zhou, J. He, M.A. Habibi, S. Melnyk, M. El-Absi, B. Han, M. Di Renzo, H.D. Schotten, F.L. Luo, T.S. El-Bawab, M. Juntti, M. Debbah, V.C.M. Leung, IEEE Commun. Surv. Tutorials, Early Access, 1 (2024). DOI: 10.1109/COMST.2024.3385908
[3] K. Ahi, S. Shahbazmohamadi, N. Asadizanjani, Opt. Lasers Eng., **104**, 274 (2018). DOI: 10.1016/j.optlaseng.2017.07.007
[4] T. Kampfrath, M. Battiato, P. Maldonado, G. Eilers, J. Nötzold, S. Mährlein, V. Zbarsky, F. Freimuth, Y. Mokrousov, S. Blügel, M. Wolf, Nat. Nanotechnol., **8** (4), 256 (2013). DOI: 10.1038/nnano.2013.43
[5] R. Rouzegar, L. Brandt, L. Nádvorník, D.A. Reiss, A.L. Chekhov, O. Gueckstock, C. In, M. Wolf, T.S. Seifert, P.W. Brouwer, G. Woltersdorf, Phys. Rev. B, **106** (14), 144427 (2022). DOI: 10.1103/PhysRevB.106.144427
[6] A.N. Yurasov, D.A. Sayfulina, T.N. Bakhvalova, Russ. Technol. J., **12** (2), 57 (2024). DOI: 10.32362/2500-316X-2024-12-2-57-66 (in Russian)
[7] T. Seifert, S. Jaiswal, U. Martens, J. Hannegan, L. Braun, P. Maldonado, F. Freimuth, A. Kronenberg, J. Henrizi, I. Radu, E. Beaurepaire, Nat. Photon., **10** (7), 483 (2016). DOI: 10.1038/nphoton.2016.91
[8] J. Pettine, P. Padmanabhan, N. Sirica, R.P. Prasankumar, A.J. Taylor, H.T. Chen, Light Sci. Appl., **12** (1), 133 (2023). DOI: 10.1038/s41377-023-01163-w
[9] C. Bull, S.M. Hewett, R. Ji, C.-H. Lin, T. Thomson, D.M. Graham, P.W. Nutter, APL Mater., **9** (9), 090701 (2021). DOI: 10.1063/5.0057511
[10] A.M. Buryakov, A.V. Gorbatova, P.Y. Avdeev, E.D. Lebedeva, K.A. Brekhov, A.V. Ovchinnikov, N.S. Gusev, E.A. Karashtin, M.V. Sapozhnikov, E.D. Mishina, N. Tiercelin, V.L. Preobrazhensky, Appl. Phys. Lett., **123** (8), 082404 (2023). DOI: 10.1063/5.0160497
[11] D. Khusyainov, S. Ovcharenko, M. Gaponov, A. Buryakov, A. Klimov, N. Tiercelin, P. Pernod, V. Nozdrin, E. Mishina, A. Sigov, V. Preobrazhensky, Sci. Rep., **11** (1), 697 (2021). DOI: 10.1038/s41598-020-80781-5

[12] M. Chen, Y. Wu, Y. Liu, K. Lee, X. Qiu, P. He, J. Yu, H. Yang, Adv. Opt. Mater., **7** (4), 1801608 (2018). DOI: 10.1002/adom.201801608
[13] G. Torosyan, S. Keller, L. Scheuer, R. Beigang, E.T. Papaioannou, Sci. Rep., **8** (1), 1311 (2018). DOI: 10.1038/s41598-018-19432-9
[14] E.T. Papaioannou, R. Beigang, Nanophotonics, **10** (4), 1243 (2021). DOI: 10.1515/nanoph-2020-0563
[15] E. Beaurepaire, G.M. Turner, S.M. Harrel, M.C. Beard, J.Y. Bigot, C.A. Schmuttenmaer, Appl. Phys. Lett., **84** (18), 3465 (2004). DOI: 10.1063/1.1737467
[16] A.M. Buryakov, A.V. Gorbatova, P.Yu. Avdeev, N.V. Bezvikonny, S.V. Ovcharenko, A.A. Klimov, K.L. Stankevich, E.D. Mishina, Tech. Phys. Lett., **48** (9), 56 (2022). DOI: 10.21883/TPL.2022.09.55084.19246].
[17] N. Kumar, R.W.A. Hendrikx, A.J.L. Adam, P.C.M. Planken, Opt. Express, **23** (11), 14252 (2015). DOI: 10.1364/OE.23.014252
[18] F.A. Zaynullin, D.I. Khusyainov, M.V. Kozintseva, A.M. Buryakov, Russ. Technol. J., **10** (3), 74 (2022). DOI: 10.32362/2500-316X-2022-10-3-74-84 (in Russian)

Translated by EgoTranslating